PCCP

In situ Environmental TEM Observation of Two-stage Shrinking of Cu_2O Islands on Cu(100) during Methanol Reduction

Journal:	*Physical Chemistry Chemical Physics*
Manuscript ID	CP-COM-10-2019-005831.R1
Article Type:	Communication
Date Submitted by the Author:	27-Dec-2019
Complete List of Authors:	Chi, Hao; University of Pittsburgh, Chemical Engineering Curnan, Matthew; University of Pittsburgh, Chemical Engineering Li, Meng; University of Pittsburgh, Chemical and Petroleum Engineering Andolina, Christopher; University of Pittsburgh, Chemical and Petroleum Engineering Saidi, Wissam; University of Pittsburgh, Chemical Engineering Veser, Götz; University of Pittsburgh, Department of Chemical and Petroleum Engineering; U.S. DOE-NETL, Yang, Judith; University of Pittsburgh, Chemical and Petroleum Engineering

COMMUNICATION

In situ Environmental TEM Observation of Two-stage Shrinking of Cu2O Islands on Cu(100) during Methanol Reduction†

Received 00th January 20xx,
Accepted 00th January 20xx

DOI: 10.1039/x0xx00000x

Hao Chi[a], Matthew T. Curnan[a,b], Meng Li[a], Christopher M. Andolina[a], Wissam A. Saidi[b], Götz Veser[a, c*], Judith C. Yang[a, d*]

The structural dynamics of Cu catalyst regeneration from Cu_2O under methanol is poorly understood. *In situ* Environmental TEM on Cu(100)-supported Cu_2O islands reveals a transition from anisotropic to isotropic shrinking during reduction. Two-stage reduction is statistically supported and explained by preferential methanol reactivity on Cu_2O nano-islands with DFT simulations.

Cu-based materials are widely used as industrial catalysts for methanol synthesis and oxidation.[1-4] The oxidation and reduction of Cu catalysts, as well as the formation of metal/oxide interfaces, play an important role in controlling the mechanisms underlying many heterogeneous catalytic reactions. They are often found to alter the reactivity and selectivity of catalytic processes, such as methanol oxidation,[5] water-gas shift,[6] and methanol synthesis.[3,7] Specifically, the transition between Cu^0 and its oxidized forms, Cu^{1+} and Cu^{2+}, during methanol oxidation or steam reforming has been shown to control selectivity towards total and partial oxidation products. Cu^0 is active towards formation of H_2 and CO_2, Cu^{1+} forms H_2O and CO, and Cu^{2+} – the least active species – produces only H_2O and CO_2.[5] However, while correlations between oxidation states and activity have been developed,[8-10] structural dynamics for this and related reactions are still largely lacking, especially at the atomic scale. This greatly hinders fundamental understanding of these processes and rational design of high-performance catalysts.

Numerous studies on the active sites of Cu-based catalysts in methanol conversion reactions have been conducted using a range of spectroscopic techniques, such as X-ray Photoelectron Spectroscopy (XPS),[10-12] Infrared Reflection Absorption Spectroscopy (IRRAS),[13] and X-ray powder Diffraction (XRD),[11, 14] as well as computational methods.[2, 15, 16] However, the active structure of Cu and the dynamic microstructural evolution of the concomitant phase transformations under methanol are little explored due to the lack of usable experimental techniques. A series of recent studies on methanol synthesis using a combination of XPS, Transmission Electron Microscopy (TEM), and theoretical modelling showed that active sites of the studied Cu/ZnO catalyst systems consist of Cu steps decorated with Zn atoms, and that these sites are stabilized by well-defined bulk defects.[1, 3, 7] However, knowledge of the structural evolution of Cu catalysts under environmental conditions at the atomic scale are lacking to-date, yet are essential to the fundamental understanding of the processes and reaction mechanisms governing these transformations.

In situ Environmental TEM (ETEM) has emerged in recent years as a powerful technique to bridge this gap. By introducing gas to the sample area, together with other external stimuli like heat, ETEM allows the study of atomic-scale structural evolution during gas-solid reactions, thus enabling new insights into reaction mechanisms and active sites of gas-solid reactions.[17-19] For example, Hansen *et al.* showed that supported Cu nanoparticles undergo dynamic reversible shape changes in response to changes in a gaseous environment.[19] Similarly, Zhou and Yang previously employed *in situ* ETEM to study nucleation, stability, and kinetics of Cu oxide island formation during Cu oxidation.[20] However, microstructural investigations of the interaction of Cu_2O with methanol, which have much broader applications especially in heterogeneous catalysis,[10, 21, 22] are absent in the literature to-date.

Here, we use *in situ* ETEM to observe the structural dynamics of Cu_2O on Cu(100) during reduction in methanol (MeOH) vapour and report an unusual a two-stage reduction process of Cu_2O islands, characterized by a transition from anisotropic to isotropic shrinking. We explain this by the preferential adsorption and dissociation of MeOH along Cu_2O surface steps, a connection that is verified by Density Functional Theory (DFT) calculations. These investigations hence yield a

[a] Department of Chemical and Petroleum Engineering, University of Pittsburgh, Pittsburgh, PA 15216, USA
[b] Department of Mechanical Engineering and Materials Science, University of Pittsburgh, Pittsburgh, PA 15216, USA
[c] Center for Energy, University of Pittsburgh, PA 15216, USA
[d] Department of Physics and Astronomy, University of Pittsburgh, Pittsburgh, PA 15216, USA

† Electronic Supplementary Information (ESI) available: ETEM data and methods, statistical methodology, and computational details. See DOI: 10.1039/x0xx00000x

new atomistic understanding of the active sites of Cu_2O during MeOH reforming reactions.

The Cu_2O nano-islands are created by oxidation of single-crystalline Cu(100) thin-film inside an ETEM (Hitachi H-9500, LaB_6 gun) with a double tilt heating holder (Hitachi). 60 nm thick single-crystalline Cu(100) films were grown on NaCl(100) substrate by *e*-beam evaporation and then transferred to TEM grids *via* a float-off method. The Cu films were annealed in 7.6×10^{-6} Torr H_2 at 650 °C to remove native oxide as well as create faceted holes. Cu_2O islands with controllable shapes were then grown in 1.5×10^{-4} Torr O_2 at 350 °C. *In situ* reduction of these Cu_2O islands were then carried out under 7.6×10^{-6} Torr MeOH vapour at 250 °C (see ESI Note 1 for details).

Fig. 1(a) shows a typical bright-field TEM image of the annealed Cu thin films with a faceted hole of (100) and (110) facets. These freshly created facets are atomically clean and well-suited for the growth of Cu_2O under O_2. Fig. 1(b) shows a typical High-Resolution TEM (HRTEM) image of a Cu_2O nano-island grown on a Cu(100) facet after *in situ* oxidation. The Cu_2O phase is confirmed by lattice spacing and electron diffraction, and has an epitaxial relationship of $Cu_2O(100)//Cu(100)$. These Cu_2O nano-islands generally have a trapezoidal shape, with a top facet of $Cu_2O(100)$ and higher-indexed side facets. These well-defined Cu_2O nano-islands formed *via in situ* oxidation are ideal for studying the reduction dynamics under MeOH.

Fig. 2, taken from the ESI movie (Movie_S1), shows a time-sequence of TEM images depicting the Cu_2O island located on the Cu(100) facet during reductive shrinking under MeOH vapour (7.6×10^{-6} Torr MeOH and 250 °C, Fig. 2a), along with the dimensional change (radius *r* and height *h*) of the Cu_2O island during the reduction (Fig. 2b). The Cu_2O nano-island has an initial height of 2.3 nm and radius (half of the width) of 5.2 nm. During the first 20 s of reduction, island structural dynamics show a pronounced anisotropic shrinking, in which the island radius strongly decreases from 5.2 to 2.3 nm. Simultaneously, island height remains virtually unchanged (minor decrease from 2.3 nm to ~2 nm). When the measured island radius roughly matches its height of 2 nm (at t = 23 s), island shrinking suddenly switches from anisotropic to isotropic, as both island height and radius decrease with similar rates until the whole island is removed at around t = 31 s.

To further confirm this two-stage shrinking behaviour, namely the transition from anisotropy to isotropy, statistical analysis of the data was conducted before fitting the change of

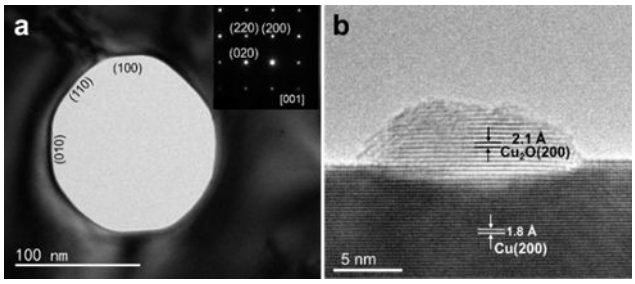

Fig 1. (a) Bright-field TEM image of a Cu(100) film after annealing and forming faceted holes at 600 °C under 7.6×10^{-6} Torr H_2; the inset shows the corresponding diffraction pattern. (b) HRTEM image of a Cu_2O nano-island on a Cu(100) facet formed at 350 °C under 1.5×10^{-4} Torr O_2.

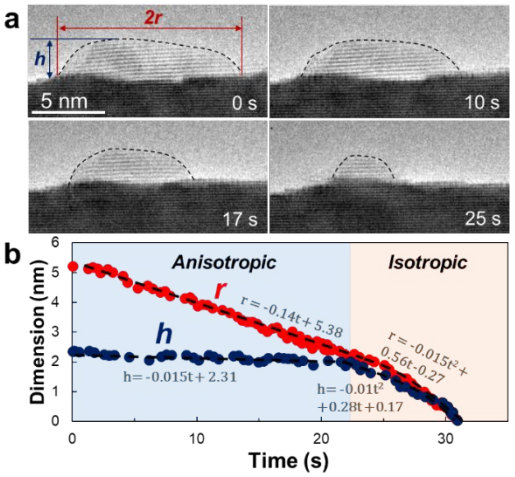

Fig 2. Reduction process of Cu_2O nano-island on Cu(100) facets at 250°C under 7.6×10^{-6} Torr MeOH vapour. (a) HRTEM image sequence depicting Cu_2O nano-island shrinking over time, the outlines of the Cu_2O islands are marked with dashed lines. (b) Change of radius (r, red, half the width) and height (h, blue) of the Cu_2O nano-island as a function of time during reduction. Dashed lines correspond to the linear fitting for anisotropic shrinking and parabolic fitting for isotropic shrinking.

island radius and height in two parts. Details of the statistical data analysis are given in ESI Note 2. As Fig. 2b and Table S8 demonstrate, both island radius and height can be fitted into linear and parabolic parts using piecewise fitting. The linear radial shrinking rate ($R_{r,l}$ = 0.14 nm/s) is an order of magnitude larger than that of island height ($R_{h,l}$ = 0.017 nm/s), indicating the anisotropy of the shrinking process. In the parabolic regime, the radial shrinking rate ($R_{r,p}$ = 0.015 nm/s^2) is close to that of height ($R_{h,p}$ = 0.011 nm/s^2), confirming isotropic dynamics. The transition dimensions between anisotropic and isotropic shrinking for radius and height are 2.2 and 2.1 nm, respectively.

We used a similar analysis for six additional Cu_2O islands and confirmed that their shrinking profiles (radius and height) again are best fitted with two regimes, namely a linear, anisotropic regime and a parabolic, isotropic regime (Fig. S1-S6).[23] Fitting parameters and determined transition dimensions for each island are summarized in Table S8. Statistical approaches described in ESI Note 2 were used to identify the transitions. Comparing the radial and vertical shrinking rates, we confirm quantitatively that radial shrinking is significantly larger than vertical shrinking in the anisotropic (linear) regime, and that both rates are similar in magnitude in the isotropic (parabolic) regime. Considering the calculated transition dimensions and rates (Table S8) of all oxide islands and shrinking regimes, in addition to the normality of fitted rate residuals (Fig. S9), inferential structural break testing confirms that the anisotropic and isotropic regimes are statistically distinct for all islands (Fig. S10). Further descriptive statistical tests confirm that anisotropic and isotropic regimes are best characterized by linear and parabolic rates of shrinking, respectively (Fig. S11).

These differences are further illustrated in Fig. 3, in which the ratio of radius and height shrinking rates (R_r/R_h) are compared for both linear and parabolic shrinking regimes. For each island, Fig. 3 shows this ratio for the parabolic ("isotropic") regime can be delimited by a 4:1 proportion favouring either

rate within measurement uncertainty. In contrast, paired linear or anisotropic regime ratios are all significantly higher than 4:1 and matched "isotropic" regime ratios within uncertainty, emphasizing the transition from anisotropy to isotropy occurs for each island. Interestingly, the island radius at the transition point from anisotropic to isotropic shrinking is slightly below ~2 nm for all islands, regardless of their initial sizes (Fig. S7).

The reduction of Cu_2O under dissociative adsorption of MeOH can be described by $Cu_2O + 2CH_3OH \rightarrow 2Cu + 2CH_3O + H_2O$, yielding Cu atoms that diffuse back to Cu substrate and water molecules that desorb from the surface.[24] Our results and this reaction suggest that the structural dynamics of Cu_2O islands on Cu(100) under MeOH are controlled by the molecular interaction between MeOH and different Cu_2O structures. As noted in ESI Note 2, fitted shrinking rate orders can be related to the number of island dimensions featuring Cu diffusion back to the substrate. Nevertheless, rate magnitudes over single island dimensions correspond to MeOH decomposition rates, and thus water desorption rates, on changing Cu_2O interfaces. Previous experimental and theoretical studies suggest that MeOH binds more strongly to Cu_2O than Cu surfaces, and that they prefer to adsorb and react with lower-coordinated Cu and O atoms.[16, 22, 23] The top surface of an epitaxial Cu_2O island has a well-defined (100) orientation (Fig. 2a); hence, O atoms on top surfaces are highly coordinated. However, island side facets are made of numerous single or multilayer atomic steps in the (100) direction, which are comprised of different combinations of Cu and O atoms that depend on surface termination. Hence, O atoms on these step edges are generally less coordinated than those at top facets. As a result, we hypothesize that MeOH would most likely adsorb and react at the side steps of an island, causing the anisotropic shrinking observed in our experiments.

When islands have similar radii and heights (below 2 nm), Cu_2O islands generally have a semi-spherical shape, in which there is no well-defined top surface. For such small nano-islands, radius magnitude equals approximately only four Cu_2O unit cell lengths. At the atomic level, interfacial Cu and O atoms should become under-coordinated, regardless of placement on the top or side facets. The MeOH molecules may favourably absorb and react with Cu and O atoms on all island surfaces proportionally, resulting in the observed isotropic shrinking. This proposed shrinking mechanism qualitatively explains the linear and parabolic shrinking rates observed in the island dimension profiles. During the anisotropic shrinking, MeOH molecules preferentially adsorb and react on the Cu_2O side facets. For constant island height, reaction area scales directly with island radius via $A_{sf} = 2\pi rh$. A_{sf} is side facet area, while r and h are the island radius and height, respectively. In contrast, during isotropic shrinking, reactions take place on the entire island surface (A_T). These reactions scale parabolically with the island radius with $A_T = n\pi r^2$, where n is a constant determined by the overall island shape and volume.

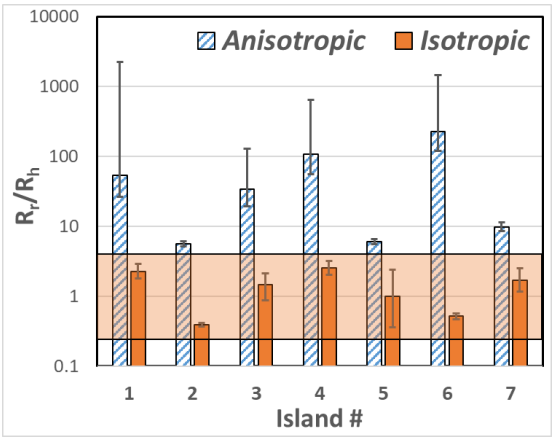

Fig 3. The ratio of radius and height shrinking rates (R_r/R_h) for anisotropic (blue with stripes) and isotropic (orange) shrinking of additional measured islands indicate similar two-stage shrinking. The isotropic shrinking region is highlighted in orange and characterized by observed R_r/R_h between 0.25 and 4.

In order to verify this hypothesis, DFT calculations were performed to compare the dissociative adsorption processes of MeOH molecules on Cu_2O(100) flat surfaces and Cu_2O(100) atomic steps. This is accomplished by comparing the adsorption and dissociation barrier energies[24] of flat and stepped interfaces using three-step models, as previously demonstrated on Cu-containing surfaces.[25-27] Adsorption energies (E_{ads}) for systems with adsorbates are set relative to the energies of corresponding surfaces without adsorbates. MeOH dissociation barriers (E_{dis}) to CH_3CO (MeO) and H adsorbate formation are set relative to undissociated MeOH E_{ads}, and are calculated using the Climbing Image Nudged Elastic Band (CI-NEB) method.[28, 29] A linear response derived Hubbard U of 9.3 eV is applied to Cu 3*d* orbitals based on previously developed techniques, which evaluate the sensitivity of results to electronic correlation correction.[30,31] Further information on all DFT results used to validate the anisotropic relationship can be found in the ESI (Note 3 and Fig. S12-S17), which shows the selected candidates for tested adsorption sites generally based on past work.[22, 32]

Fig. 4 shows the energetically most favourable, O-terminated flat Cu_2O(100) (brown) and the stepped Cu_2O(100){100} (green) interfaces used to validate experimental anisotropic shrinking. Simulation of these dissociated MeO and H adsorbate systems, as well as the reaction processes to achieve these from corresponding adsorbate-free systems, was completed using separate structures. E_{ads} and E_{dis} for flat Cu_2O(100) surfaces that either omit or consider (in parenthesis, associated content in light brown) Hubbard U agree within 0.13 eV or less, while the E_{dis} of the most favourable stepped Cu_2O(100){100} and flat surface systems not considering electronic correlation agree within 0.06 eV. These differences are small compared to the difference (0.69 eV) between MeOH E_{ads} on the most favourable flat (-1.55 eV) and stepped (-2.24 eV) Cu_2O(100) surfaces. As shown in Fig. S12-S15, these most favourable structures were resolved by testing different relative MeO and H adsorbate site configurations on Cu and O terminated interfaces. This evaluation of candidate structures indicated that MeO and H adsorption is strongly favoured on stepped Cu_2O(100) structures. These results indicate an initial selective reaction of MeOH with Cu_2O island side facets, supporting our experimental observation of initial anisotropic island shrinking.

To our knowledge, this is the first in situ observation of a

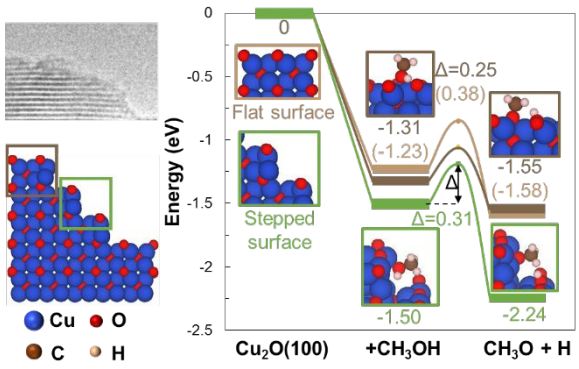

Fig 4. DFT calculated adsorption (E_{ads}) and dissociation barrier (E_{dis}) energies of methanol for flat $Cu_2O(100)$ (brown) and stepped $Cu_2O(100)\{100\}$ (green) candidate systems, considering the effects of Hubbard U inclusion for flat $Cu_2O(100)$ in parenthesis and light brown. Cu, O, C, and H atoms are blue, red, brown, and white, respectively.

two-stage reduction process of a metal oxide island that transitions from anisotropic to isotropic shrinking, based on a structural break identifying statistical test to identify and justify the presence of such different kinetic regimes. We propose that the preferential dissociative adsorption of methanol molecules on $Cu_2O(100)$ atomic steps compared to flat terraces results in the initial anisotropic shrinking from island side facets, as further verified by DFT calculations. This explanation is furthermore consistent with the fact that the anisotropic regime can be described with a linear rate law for the radius, while the isotropic regime shows a parabolic behaviour.

Our study produced new atomistic insights on the active sites of Cu_2O nano-islands during reductive shrinking under methanol. Our results suggest that stepped surfaces on very small Cu_2O nanoparticles (radius < 2 nm) significantly enhance the rates of methanol oxidation on such nanoparticles, yielding a clear target for the rational design of optimized nano-catalysts for this reaction. Furthermore, we demonstrate that the combination of *in situ* ETEM experiments with statistical analysis and DFT computational studies forms a powerful approach towards gaining fundamental insights into catalytic reactions. Given the increasing access to ETEM instrumentation, our understanding of heterogeneous catalysis and related gas-solid phenomena is poised to make significant advances.

Conflicts of interest

The authors have no conflicts to declare.

Acknowledgments

This work is supported by the National Science Foundation CBET-1264637, DMR-1410055, and DMR-1508417. Experiments were performed at NFCF and theoretical calculations were performed using the Extreme Science and Engineering Discovery Environment and the Center for Research Computing, University of Pittsburgh.

Notes and references

1. M. Behrens, F. Studt, I. Kasatkin, S. Kuhl, M. Havecker, F. Abild-Pedersen, S. Zander, F. Girgsdies, P. Kurr, B. L. Kniep, M. Tovar, R. W. Fischer, J. K. Norskov and R. Schlogl, *Science*, 2012, **336**, 893-897.
2. L. C. Grabow and M. Mavrikakis, *ACS Catalysis*, 2011, **1**, 365-384.
3. S. Kuld, M. Thorhauge, H. Falsig, C. F. Elkjaer, S. Helveg, I. Chorkendorff and J. Sehested, *Science*, 2016, **352**, 969-974.
4. F. Studt, M. Behrens, E. L. Kunkes, N. Thomas, S. Zander, A. Tarasov, J. Schumann, E. Frei, J. B. Varley, F. Abild-Pedersen, J. K. Nørskov and R. Schlögl, *ChemCatChem*, 2015, **7**, 1105-1111.
5. S. R. González Carrazán, R. Wojcieszak, R. M. Blanco, C. Mateos-Pedrero and P. Ruiz, *Appl. Catal., B*, 2015, **168-169**, 14-24.
6. M. S. Spencer, *Top. Catal.*, 1999, **8**, 259-266.
7. R. van den Berg, G. Prieto, G. Korpershoek, L. I. van der Wal, A. J. van Bunningen, S. Laegsgaard-Jorgensen, P. E. de Jongh and K. P. de Jong, *Nat Commun*, 2016, **7**, 13057.
8. I. E. Wachs and R. J. Madix, *J. Catal.*, 1978, **53**, 208-227.
9. B. A. Sexton, *Surf. Sci.*, 1979, **88**, 299-318.
10. J. N. Russell, S. M. Gates and J. T. Yates, *Surf. Sci.*, 1985, **163**, 516-540.
11. H. Chi, C. M. Andolina, J. Li, M. T. Curnan, W. A. Saidi, G. Zhou, J. C. Yang and G. Veser, *Appl. Catal., A*, 2018, **556**, 64-72.
12. T. J. Lawton, G. Kyriakou, A. E. Baber and E. C. H. Sykes, *ChemCatChem*, 2013, **5**, 2684-2690.
13. S. D. Senanayake, P. J. Ramírez, I. Waluyo, S. Kundu, K. Mudiyanselage, Z. Liu, Z. Liu, S. Axnanda, D. J. Stacchiola, J. Evans and J. A. Rodriguez, *J. Phys. Chem. C*, 2016, **120**, 1778-1784.
14. J. Y. Kim, J. A. Rodriguez, J. C. Hanson, A. I. Frenkel and P. L. Lee, *J. Am. Chem. Soc.*, 2003, **125**, 10684-10692.
15. S. Sun, Y. Wang and Q. Yang, *Appl. Surf. Sci.*, 2014, **313**, 777-783.
16. S. Sakong and A. Gross, *J. Phys. Chem. A*, 2007, **111**, 8814-8822.
17. L. Zou, J. Li, D. Zakharov, E. A. Stach and G. Zhou, *Nat Commun*, 2017, **8**, 307.
18. W. Zhu, J. P. Winterstein, W. D. Yang, L. Yuan, R. Sharma and G. Zhou, *ACS Nano*, 2017, **11**, 656-664.
19. P. L. Hansen, J. B. Wagner, S. Helveg, J. R. Rostrup-Nielsen, B. S. Clausen and H. Topsoe, *Science*, 2002, **295**, 2053-2055.
20. J. C. Yang and G. Zhou, *Micron*, 2012, **43**, 1195-1210.
21. R. Ryberg, *J. Chem. Phys.*, 1985, **82**, 567-573.
22. Z. Besharat, J. Halldin Stenlid, M. Soldemo, K. Marks, A. Onsten, M. Johnson, H. Ostrom, J. Weissenrieder, T. Brinck and M. Gothelid, *J. Chem. Phys.*, 2017, **146**, 244702.
23. M. Bowker, *Chem. Soc. Rev.*, 2007, **36**, 1656-1673.
24. Q. Zhu, W. A. Saidi and J. C. Yang, *J Phys Chem Lett*, 2016, **7**, 2530-2536.
25. C. M. Andolina, M. T. Curnan, Q. Zhu, W. A. Saidi and J. C. Yang, *Microsc. Microanal.*, 2017, **23**, 920-921.
26. Q. Zhu, W. A. Saidi and J. C. Yang, *J. Phys. Chem. C*, 2014, **119**, 251-261.
27. Q. Zhu, W. A. Saidi and J. C. Yang, *J. Phys. Chem. C*, 2017, **121**, 11251-11260.
28. G. Henkelman, B. P. Uberuaga and H. Jónsson, *J. Chem. Phys.*, 2000, **113**, 9901-9904.
29. G. Henkelman and H. Jónsson, *J. Chem. Phys.*, 2000, **113**, 9978-9985.
30. M. Cococcioni and S. de Gironcoli, *Phys. Rev. B*, 2005, **71**, 035105.
31. M. T. Curnan and J. R. Kitchin, *J. Phys. Chem. C*, 2015, **119**, 21060-21071.
32. Z. Riguang, L. Hongyan, L. Lixia, L. Zhong and W. Baojun, *Appl. Surf. Sci.*, 2011, **257**, 4232-4238.